

Permanent Magnet Synchronous Generator Connected to a Grid via a High Speed Sliding Mode Control

Omokhafa J. Tola ^{a,1,*}, Edwin A. Umoh ^{b,2}, Enesi A. Yahaya ^{a,3}, Osinowo E. Olusegun ^{c,4}

^a Department of Electrical and Electronic Engineering, Federal University of Technology, Minna, Nigeria

^b Department of Electrical and Electronic Engineering, Federal Polytechnic, Kaura Namoda, Nigeria

^c Nigeria Television Authority, Channel 10, Lagos, Nigeria

¹ omokhafa@futminna.edu.ng; ² eddyumoh@gmail.com; ³ enesi.asizehi@futminna.edu.ng;

⁴ olusegunosinowo1@gmail.com

* Corresponding Author

ARTICLE INFO

ABSTRACT

Article history

Received April 03, 2022

Revised May 14, 2022

Accepted June 12, 2022

Keywords

Permanent magnet

Synchronous generator;

Optimum variable speed;

Sliding mode control;

Wind power generation has recently received a lot of attention in terms of generating electricity, and it has emerged as one of the most important sources of alternative energy. Maximum power generation from a wind energy conversion system (WECS) necessitates accurate estimation of aerodynamic torque and system uncertainties. Regulating the wind energy conversion system (WECS) under varying wind speeds and improving the quality of electrical power delivered to the grid has become a difficult issue in recent years. A permanent magnet synchronous generator (PMSG) is used in the grid-connected wind-turbine system under investigation, followed by back-to-back bidirectional converters. The machine-side converter (MSC) controls the PMSG speed, while the grid-side converter (GSC) controls the DC bus voltage and maintains the unity power factor. The control approach is second-order sliding mode controls, which are used to regulate a nonlinear wind energy conversion system while reducing chattering, which causes mechanical wear when using first-order sliding mode controls. The sliding mode control is created using the modified super-twisting method. Both the power and control components are built and simulated in the same MATLAB/Simulink environment. The study successfully decreased the chattering effect caused by the switching gain owing to the high activity of the control input.

This is an open-access article under the [CC-BY-SA](https://creativecommons.org/licenses/by-sa/4.0/) license.



1. Introduction

The demand for electrical energy is growing rapidly. But the attention is geared toward clean and renewable energy. There are many renewable energy resources used in electric power generation. These energy resources are photovoltaic, wind, biomass, fuel cell, and tidal [1]–[3]. Wind as a promising energy source is freely available, omnipresent, and environmentally friendly. It is highly reliable and cost-effective. These features made wind power generation capability to have been grown rapidly, with an average annual growth of 30% in the world energy resources over the last decade [4][5]. The wind turbine and electric generator are the major components used in electric energy wind generation. It could be used standalone or fed to the grid network via a suitable power electronic converter.

The wind turbine could either operate at fixed or variable speed. In fixed speed operation, the system operates at a constant speed even if the wind speed varies. However, the system is simple and less expensive. But the operation suffers from low energy capture, poor power quality, and mechanical stress. The variable speed wind turbine generator is of high efficiency due to the high energy captured from the wind over a wide range of wind speeds and possesses a good power quality. The topology has the capability to regulate the power factor either by overriding or generating reactive power [5], [6].

A wind generator normally changes the mechanical energy of the wind into electrical energy. But there are different kinds of wind generators discussed in the literature, such as Induction generators, Double fed Induction generators (DFIG), and Permanent Magnet Synchronous Generators (PMSG). Squirrel Cage Induction Generator (SCIG) is a well known generator applied for constant wind turbine speed. The rotor of the turbine and the stator is directly connected to the grid via a capacitor bank. The major drawback of the type is that higher mechanical stress, low efficiency, minimal capability to control active and reactive power, and requires higher gearbox maintenance [7]–[10]. Similarly, DFIG is for variable speed but results in the reduction of mechanical stress, and power oscillation has the capability of MPPT for speed controller and has the flexibility to control active and reactive power. However, DFIG uses brushes that reduces the robustness and leads to extra maintenance cost that SCIG [11]–[13].

However, in PMSG, its reactive power can be controlled and can be applied to supply reactive to other items of the power system. But the generators are more costly and prone to failures than the induction generators. The advantages over the electrically excited generator are higher efficiency, higher reliability due to the absence of slip rings, and a higher power-to-weight ratio. The major drawback of PMSG is the high cost of PMs material and demagnetization at high temperatures. However, the cost of PMs material has been reduced in recent times due to the high performance and attractiveness in research on PMs [13], [14], [15]–[17].

The control of a wind generator is complex due to its electromechanical system. In the field of engineering, linear controllers are widely used, owing to their uncomplicatedness and reliability. However, their parameters are typically tuned with a projected linearized model. But the control performance cannot be assured throughout the transient of the wind turbine energy system. These motivate researchers to pay much attention to the design of the controller to ensure a good control performance robustness to parameters uncertainties and disturbances. The following control strategies are analyzed. Field-oriented control (FOC) is widely used in grid-connected wind energy control systems [18], [19]. The performance normally means deviation of the machine parameters (resistance and inductance) from the value used in the control system [20]–[22]. Feedback linearization is another control technique based on coordinate transformation using the differential geometry theory. But the technique does not guarantee robustness in disturbance present [23]. Direct torque control (DTC) is a technique with the advantages of simplicity and insensitivity to parameter variation. It directly controls the machine torque and stator flux by selecting the voltage vector using stator flux and torque transformation. The drawback of the technique is poor performance during starting and low-speed operation and sensitivity to the disturbance in the case of PI controller [24]–[26]. Direct power control (DPC) is based on DTC. Its control systems are less complicated and robust against the parameters variation of the machine. However, its switching frequency varies considerably with the active and reactive power variations [27], [28]. Sliding mode control (SMC) is the most robust control technique among the analyzed strategies with uncertainties and parameter variations. Simple in its implementation, good robustness, and high in disturbance rejection [26], [29]–[31].

In this study, a second-order SMC with a modified super-twisting algorithm for variable speed wind turbine based on a permanent magnet synchronous generator (PMSG) grid-connected is analyzed. Higher-order sliding mode controllers (SMCs) in wind energy conversion systems are being investigated. While SMCs show promise in wind energy conversion systems for speed control (because of their ability to deal with the extremely nonlinear nature of wind), they are constantly threatened by chattering. This study begins with a discussion of SMC theory and higher-order SMCs based on the modified super-twisting algorithm used to generate a second-order SMC. The modified

super-twisting procedure is then used to model PMSG for a WECS, which is analyzed using d-q reference frame transformation methods.

2. Modeling of a Wind Energy Conversion System

This model consists of the generation side and the Grid side (Fig. 1). The focus of this study is on the control of the power of the generator side.

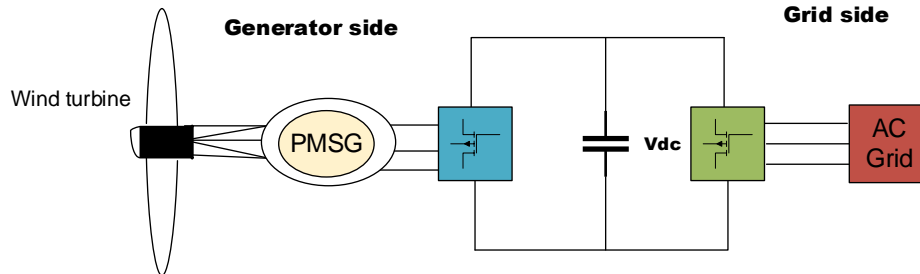


Fig. 1. Wind energy conversion based on PMSG

2.1. Modeling of the Wind Turbine

The wind energy conversion system converts the kinetic energy of the wind into mechanical power using the wind turbine. The kinetic energy and the power, which is the input power to the wind turbine, can be expressed as [32]. The energy and power of the wind can be expressed as (1) and (2)

$$E_m = \frac{1}{2}mv^2 \quad (1)$$

where m is the air mass expressed as $m = \rho Av$

$$P_w = 0.5\rho\pi R^2 V_w^3 \quad (2)$$

Since the mechanical power extracted from the wind depend on the power coefficient of the turbine and is usually provided by the manufacturer of WT. therefore, the output power is given as

$$P_m = 0.5\rho\pi R^2 C_p(\lambda, \beta) V_w^3 \quad (3)$$

Where ρ is the air density, R is the radius of the wind turbine, V_m is the wind speed, $C_p(\lambda, \beta)$ is the power coefficient, λ is the tip speed ratio, and β is the turbine blade pitch.

Therefore, the power coefficient and the tip speed ratio are expressed as

$$C_p(\lambda, \beta) = c_1 \left(\frac{c_2}{\lambda_i} - c_3\beta - c_4 \right) e^{\frac{-c_5}{\lambda_i}} + c_6\lambda \quad (4)$$

$$\lambda_i^{-1} = (\lambda + 0.08\beta)^{-1} - 0.035(1 + \beta^3)^{-1} \quad (5)$$

$$\lambda = \frac{\Omega_h R}{V_m} \quad (6)$$

This equation reveals that the optimum tip speed ratio can be obtained by varying the rotor speed where Ω_h is the low-speed shaft rotational speed. Therefore, the instantaneous change of the wind speeds the speed necessitates the operation at MPPT. A robust controller must be employed to regulate the speed of the rotor in order to maximize the power as a result of the change in the wind speed.

The output power capture by the WT with respect to the speed is shown in Fig. 2, which has one optimal point. By considering some values, the wind power can be regulated by comfortably fine-tuning the speed ratio or tip speed.

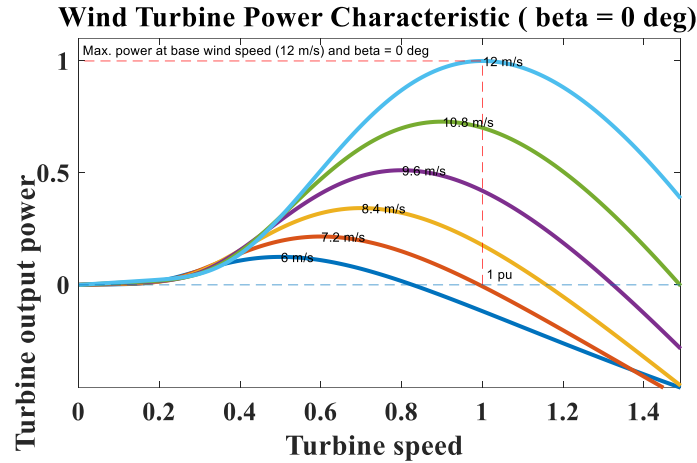


Fig. 2. Wind turbine power characteristics

2.2. Modeling of the PMSG and DC-DC converter

The PMSG is modeled under the following simplifying assumption: sinusoidal distribution of the stator winding, electric and magnetic symmetry, negligible iron losses, and unsaturated magnetic circuit. By neglecting the homo polar voltage, V_0 , which is by virtue of symmetry, the voltage equation in the d-q reference frame can be expressed as [33]–[35].

$$V_d = -R_s i_d - L_d \frac{di_d}{dt} + \omega_e L_q i_q \quad (7)$$

$$V_q = -R_s i_q - L_q \frac{di_q}{dt} + \omega_e L_d i_d + \omega_e \lambda_m \quad (8)$$

Where ω_e is the stator pulsation and is directly proportional to the shaft rotational speed, which depends on how the generator interacts mechanically.

$$\omega_e = \rho \Omega_h \quad (9)$$

and λ_m is the permanent magnet flux. The electromagnetic torque equation of the generator excited by the turbine can be given as [36]

$$T_L = \frac{1}{2} N_p [\lambda_m i_q + (L_d - L_q) i_q i_d] \quad (10)$$

But for surface-mounted PMSG, the electromagnetic torque is expressed as

$$T_L = \frac{1}{2} N_p \lambda_m i_q \quad (11)$$

And the overall equivalent model of PMSG based wind turbine is

$$\begin{cases} \frac{di_d}{dt} = -\frac{R_s}{L} i_d + \frac{N_p}{2} i_q \omega_r - \frac{1}{L} v_d \\ \frac{di_q}{dt} = -\frac{R_s}{L} i_q + \frac{N_p}{2} (i_d - \frac{\lambda_m}{L}) \omega_r - \frac{1}{L} v_q \\ \frac{d\omega_r}{dt} = \frac{T_m}{J} - \frac{k_i i_q}{J} - \frac{B \omega_r}{J} \end{cases} \quad (12)$$

where V_d, V_q and i_d, i_q and L_d, L_q are d, q axis stator voltage, current, and inductances, respectively. λ_m is the permanent magnet leakage flux and ω_e is the reference frame speed [37][38]. The state input vector can be expressed as

$$\begin{cases} X = [x_1(t) x_2(t)]^T = [i_d(t) i_q(t)]^T \\ U = [V_d V_q]^T \end{cases} \quad (13)$$

The grid-connected PMSG state model is obtained in the form as

$$\begin{cases} \dot{X} = \begin{bmatrix} \frac{-R}{L_d} x_1 + \rho \frac{L_q}{L_d} x_2 \Omega_h \\ \frac{-R}{L_d} x_2 - \rho \frac{L_d x_1 - \lambda_m}{L_q} \Omega_h \end{bmatrix} + \begin{bmatrix} \frac{-1}{L_d} & 0 \\ 0 & \frac{-1}{L_d} \end{bmatrix} \\ y = T_G = \rho \lambda_m x_2 \end{cases} \quad (14)$$

The electromagnetic torque is given as

$$T_G = \frac{-3}{2} N_p \rho \lambda_m i_q \quad (15)$$

and the PMSG mechanical equation is given as

$$J \frac{d\Omega_h}{dt} = T_i - T_G - f \Omega_h \quad (16)$$

The PMSG parameters are given in Table 1,

Table 1. System parameters of the PMSG [38]

Parameter	Value
No of phases	3
Rotor type	Round
Phase resistance	0.15 ohm
Inductance	5.3mH
Moment of Inertia (J)	0.016 (kgm ²)
Number of pole pairs	4
Rated speed	200 (rpm)

2.3. The Boost Converter

The power from the generator PMSG is transferred to the grid via the converters. The two three-phase voltage source converters in the back-to-back configuration with a DC link have been boosted with a DC-DC converter. The generator-side converter operates as a rectifier; the DC-DC boost converter whose role is to boost the energy stored in the DC link. The boost converter controller stabilizes the voltage V_{dc} on the DC link and synchronizes using (MPPT-SMC and P & O approaches) to control the grid-side converter output voltages and current established in the grid system.

The boost converter is designed properly after the generation of power from PMSG. The input and output voltage and current of the converter at steady-state operation are given as [39]

$$V_0 = \frac{V_{dc}}{(1-D)} \quad (17)$$

$$I_0 = I_{dc}(1-D) \quad (18)$$

where D is the duty cycle.

$$\frac{dI_{dc}}{dt} = \frac{R_{dc}}{L_{dc}} I_{dc} + \frac{1}{L_{dc}} V_T - \frac{(1-D)}{L_{dc}} V_{dc} \quad (19)$$

$$\frac{dV_T}{dt} = \frac{1}{C_0} I_T - \frac{1}{C_0} I_{dc} \quad (20)$$

where R_{dc} and L_{dc} are resistance and inductance of the boost converter. V and I_T are voltage and current of the output of the rectifier while V_{dc} is the DC link voltage. The grid side converter model in the d - q reference frame can be presented as

$$\begin{cases} \frac{dI_{gd}}{dt} = \left[\frac{v_{id}}{L_f} - \frac{R_f}{L_f} I_{gd} + \omega_g I_{gq} - \frac{v_{gd}}{L_f} \right] \\ \frac{dI_{gq}}{dt} = \left[\frac{v_{iq}}{L_f} - \frac{R_f}{L_f} I_{gq} + \omega_g I_{gd} - \frac{v_{gq}}{L_f} \right] \end{cases} \quad (21)$$

where R_f and L_f resistance and inductance of the grid side filter, respectively. v_{id} and v_{iq} are inverter output voltage. v_{gd} and v_{gq} are grid voltage. The grid's active and reactive power can be expressed as

$$\begin{cases} P_g = \frac{3}{2} [v_{gd} \times I_{gd} + v_{gq} \times I_{gq}] \\ Q_g = \frac{3}{2} [v_{gq} \times I_{gd} + v_{gd} \times I_{gq}] \end{cases} \quad (22)$$

where v_{gd} and v_{gq} are the grid d - q axis voltage

3. Sliding Mode Controller Design

Chattering is the main drawback of traditional sliding mode control. Several ways are introduced to reduce chattering. High order sliding mode (HOSM) [40] is one of the attractive chattering-free sliding modes. However, the fundamental issue in implementing the HOSM algorithm's complexity. One of the HOSM modes that does not require additional information is the super-twisting sliding mode (STMC) [41][42].

In general, an n -th order sliding controller necessitates an understanding of the $(n-1)$ -th order time derivative. As a result, an r -th order sliding mode can be established.

$$\sigma = \dot{\sigma} = \ddot{\sigma} = \dots = \sigma^{n-1} = 0 \quad (23)$$

The super-twisting controller, which is one of several second-order sliding mode controllers, has the advantage of not requiring knowledge. Using the same access information, the super-twisting controller can be utilized instead of the first-order (standard) sliding mode.

The necessity for more information is the main issue with the higher order. The development of an n th order controller, in particular, necessitates an understanding of $\dot{\sigma}, \ddot{\sigma}, \ddot{\sigma}, \dots, s^{(n-1)}$. The proposed MST algorithm replaces the super-twisting approach to solve this problem. The MST algorithm, which is utilized in second-order SMC techniques, requires only one sliding surface.

The Proposed Controller is designed using Lyapunov function. The following function offers finite time convergence at the origin (0,0):

$$\ddot{\sigma} = \phi(t, \dot{\sigma}) + \tau(t, \sigma, \dot{\sigma})u; \quad (24)$$

and the control $u(t)$ is the sum of two components.

$$u_1(t) = A_1 * B_1 \quad (25)$$

Where

$$A_1 = k_1 |e_1|^{1/2} \quad (26)$$

$$B_1 = \text{sign}(e_1) + k_2 \text{sign}(e_1) + \int k_1 \text{sign}(e_1) \quad (27)$$

$$u_2(t) = k_2 |e_1|^{1/2} \text{sign}(e_1) \quad (28)$$

Where k_1 and k_2 are positive design constant e_1 is the sliding manifold and $|e_1|$ is a bounded command value. In addition, when compared to the ST algorithm, the term B_1 lowers substantial chattering.

3.1. D-Axis Controller Design

The goal of the d-axis controller is to keep the d-axis current of the generator to zero, both $s_d(t)$ and $\dot{s}_d(t)$ must be zero.

The sliding mode surface for (12) is defined as

$$\begin{cases} s_d(t) = [i_d(t) - i_d^*(t)] = 0 \\ s_q(t) = [i_q(t) - i_q^*(t)] = 0 \\ s_{\omega r}(t) = [\omega_r(t) - \omega_r^*(t)] = 0 \end{cases} \quad (29)$$

Where $i_q^*(t)$ are the reference values for the d-axis and q-axis, and the speed reference is $\omega_r^*(t) = i \frac{v\lambda}{R}$ where i is the fixed drive train multiplier ratio, the following inequalities ensure that the trajectories remain directed toward their respective state sliding surface for the reachability criterion. And the d-axis controller must satisfy the inequalities in (30)

$$\begin{cases} s_d(t)\dot{s}_d(t) \leq 0 \\ s_q(t)\dot{s}_q(t) \leq 0 \\ s_{\omega r}(t)\dot{s}_{\omega r}(t) \leq 0 \end{cases} \quad (30)$$

$$\dot{s}_d = \frac{1}{L_d} [-R_s i_d + N_p \omega_r L_d L_q - v_d] - \frac{di_{dref}}{dt} \quad (31)$$

$$\ddot{s}_d = -\frac{R_s}{L_d} \frac{di_d}{dt} + N_p \frac{d\omega_r}{dt} i_q + N_p \frac{di_q}{dt} \omega_r - \frac{1}{L_d} \frac{dv_d}{dt} - \frac{d^2 i_{dref}}{dt^2} \quad (32)$$

The control law is applied by

$$v_d = \Delta v_d + v_d eq \quad (33)$$

Where Δv_d is the control term and $v_d eq$ is an equivalent control term when $\dot{s}_d = 0$ and (33) composed of switching control terms which converge the sliding surface to zero in finite time with the help of MST algorithm. This speeds up the system response and reduces the steady-state error.

$$\Delta v_d = k_1 \sqrt{|e_1|} \text{sign}(e_1) + k_2 \text{sign}(e_1) + \int k_1 \text{sign}(e_1) dt \quad (34)$$

and the control equivalent can be determined as

$$v_d eq(t) = -v_{d0} \text{sign}(s_d(t)) \quad (35)$$

where

$$v_{d0}(t) > \left| \frac{1}{L_d} [-R_s i_d + N_p \omega_r L_d L_q - v_d] \right| \quad (35)$$

The d-axis control law should ensure that the trajectory of $i_d(t)$ is directed towards the surface, that it stays there even when bounded disturbances are present.

3.2. Q-Axis Current Controller Design

The q-axis control design can be done using the same method as the d-axis control design. Taking into account the reachability condition inequality and rewriting it using PMSG dynamics.

$$\dot{s}_q = \frac{1}{L_q} [-R_s i_q + N_p \omega_r (L_d i_d - \lambda_m) - v_q] - \frac{di_{qref}}{dt} \quad (37)$$

$$\ddot{s}_q = -\frac{R_s}{L_q} \frac{di_q}{dt} + N_p \frac{d\omega_r}{dt} \left(i_q - \frac{\lambda_m}{L_q} \right) + N_p \frac{di_q}{dt} \omega_r - \frac{1}{L_q} \frac{dv_q}{dt} - \frac{d^2 i_{qref}}{dt^2} \quad (38)$$

and the control law is given as

$$v_q = \Delta v_q + v_q eq \quad (39)$$

where

$$\Delta v_q = k_1 \sqrt{|e_2|} \text{sign}(e_2) + k_2 \text{sign}(e_2) + \int k_1 \text{sign}(e_2) dt \quad (40)$$

$$v_q eq(t) = -v_{q0} \text{sign}(s_q(t)) \quad (41)$$

where

$$v_{q0}(t) > \left| \frac{1}{L_q} [-R_s i_q + N_p \omega_r (L_d i_d - \lambda_m) - v_q] \right| \quad (42)$$

3.3. Speed Controller Design

The speed reference $\dot{s}_{\omega_r}(t)$ can be rewritten using the same procedure as for the d- and q-axis controls and ensuring that inequality (30) is satisfied. The control variable $\dot{\omega}_r(t)$ is changed to precisely compensate for rotational speed variations based on the wind input, which is the desired consequence of this controller.

$$\dot{s}_{\omega_r}(t) = \frac{1}{k_t} \left[T_m - B \omega_r(t) - J \frac{d\dot{\omega}_r(t)}{dt} \right] \quad (43)$$

where the switching portion can be expressed as

$$\omega_r eq(t) = -\omega_{r0} \text{sign}(s_{\omega_r}(t)) \quad (44)$$

where

$$\omega_{r0} = \left| \frac{1}{k_t} \left[T_m - B \omega_r(t) - J \frac{d\dot{\omega}_r(t)}{dt} \right] \right| \quad (45)$$

3.4. Gridside Converter Control

The grid side converter is responsible for managing the power injection into the grid via voltage-oriented control (VOC) based on enhanced Sliding Mode Control [29]. The main control circuit has two control loops: an outer loop that adjusts the dq-axis current and an inner loop that keeps the DC-link voltage at a constant reference value.

The GSC equations in the dq-axis reference frame, with the grid voltage vector, can be presented as:

$$\begin{cases} v_{gd} = R_g i_{gd} + L_{gd} \frac{di_{gd}}{dt} - L_{gq} \omega_g i_{gq} + v_{gd} \\ v_{gq} = R_g i_{gq} + L_{gq} \frac{di_{gq}}{dt} - L_{gd} \omega_g i_{gd} \\ C \frac{dv_{dc}}{dt} = i_{gdc} - \frac{3}{2} \left(\frac{v_{gd}}{v_{dc}} i_{gd} \right) \end{cases} \quad (46)$$

where i_{gd} and i_{gq} are d - q axis grid-side current, respectively, R_f is filter resistance, L_f filter inductance V_{id} , V_{iq} are inverter d - q axis voltage and Ω_g Grid frequency. And the active and reactive power is expressed as

$$\begin{cases} P = \frac{3}{2} (V_{gd} i_{gd} + V_{gq} i_{gq}) \\ Q = \frac{3}{2} (V_{gd} i_{gq} - V_{gq} i_{gd}) \end{cases} \quad (47)$$

The voltage equations from Eq. (46) can be reformulated to be as:

$$\begin{cases} \frac{di_{gd}}{dt} = \frac{1}{L_{gd}} (-R_f i_{gd} + L_{gq} \omega_g i_{gq} - v_{gd} + v_{gcd}) \\ \frac{di_{gq}}{dt} = \frac{1}{L_{gq}} (-R_f i_{gq} + L_{gd} \omega_g i_{gd} + v_{gcq}) \end{cases} \quad (48)$$

The following sliding surfaces s_1 and s_2 have been chosen to control grid current components i_{gd} , i_{gq}

$$\begin{cases} s_{g1} = i_{gd}^* - i_{gd} \\ s_{g2} = i_{gq}^* - i_{gq} \end{cases} \quad (49)$$

where i_{gd}^* , i_{gq}^* are the desired dq -axis currents. Thus, the time derivative in (49) can be calculated using (48)

$$\begin{cases} \frac{ds_{g1}}{dt} = \frac{di_{gd}^*}{dt} - \frac{1}{L_{gd}} (-R_f i_{gd} + L_{gq} \omega_g i_{gq} - v_{gd} + v_{gcd}) \\ \frac{ds_{g2}}{dt} = \frac{di_{gq}^*}{dt} - \frac{1}{L_{gq}} (-R_f i_{gq} + L_{gd} \omega_g i_{gd} + v_{gcq}) \end{cases} \quad (50)$$

$$\begin{cases} v_{gcd}^* = \Delta v_{gcd} + v_{gcd} eq \\ v_{gcq}^* = \Delta v_{gcq} + v_{gcq} eq \end{cases} \quad (51)$$

And the overall control system configuration is shown in Fig. 3.

4. Results and Discussion

To analyze the performance of the proposed sliding mode controller, the PMSG was simulated in the MATLAB/Simulink environment. The system's parameters are tabulated in Table 1. Fig. 4 shows the wind variation with a maximum of 10 m/s and a minimum of 5 m/s, which is the input to the PMSG wind energy system. This demonstrates the effectiveness of the control design as a result of its highly nonlinear nature and wind speed range. The SMC controller manages to ensure speed tracking.

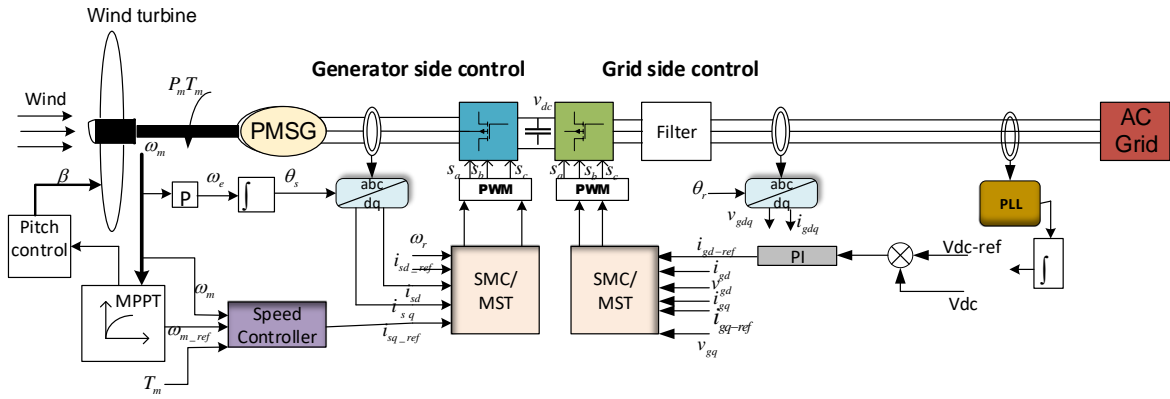


Fig. 3. Control system configuration of the PMSG

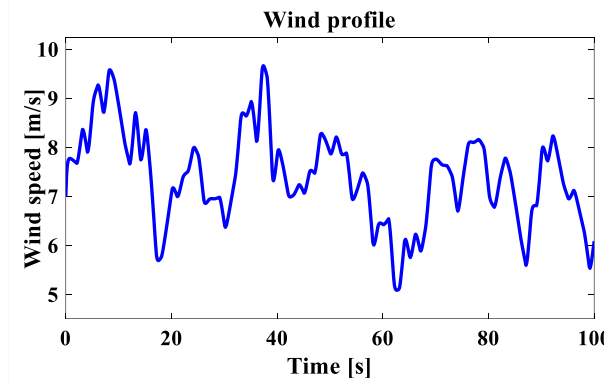


Fig. 4. Wind speed variation

Fig. 4 and Fig. 6 demonstrate the variations in wind speed and rotor speed, respectively. The power coefficient, rotational shaft speed, and power profile are shown in Fig. 5, Fig. 6, and Fig. 7, respectively. The performance is comparable to those with an observed good performance is comparable to those with reference (Fig. 8). The output power and torque of a wind turbine are proportional to the rotor speed.

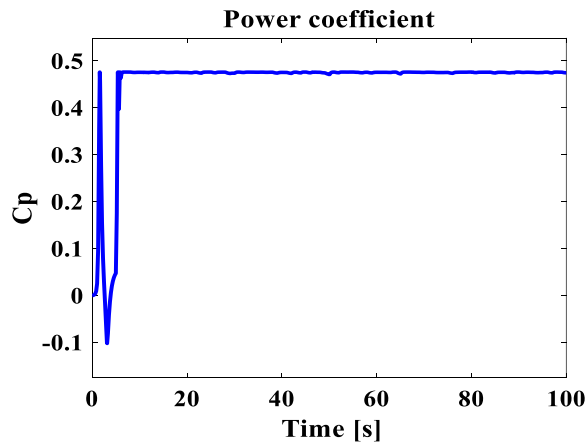


Fig. 5. Power coefficients of the wind turbine

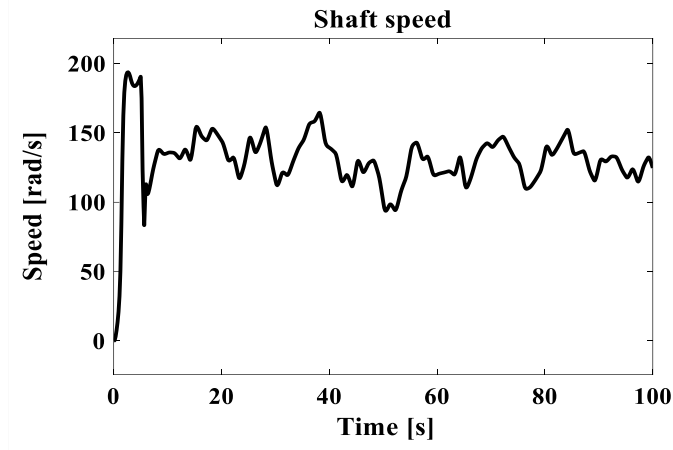


Fig. 6. Rotational shaft speed

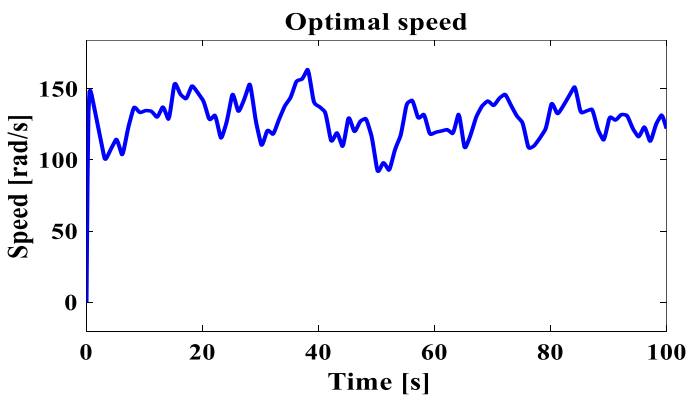


Fig. 7. Optimal shaft speed

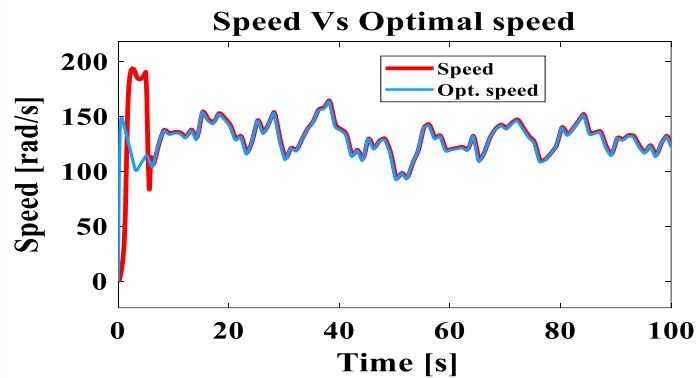


Fig. 8. The plot of reference speed and shaft speed

Fig. 9 also shows the chattering about the reference with the sliding mode control as the d-axis current accurately tracks the reference value at $i_d(t) = 0$. The implementation of the sliding mode controller is based on the rotational shaft speed of the generator and the optimal speed shown in Fig. 11, which accurately tracks the reference speed with a very significant chattering effect. The maximum power is captured through the MPPT control strategy of the sliding mode controller. Fig. 10 shows the power coefficient C_p correspond to the wind profile in Fig. 4 and the result, which is the most important regard of MPPT. The value of C_p held near at the C_{pmax} of 0.47 as shown despite the variation in the wind and the uncertainties. The tip speed ratio is kept at its optimal value of 7 despite wind variation, as seen in Fig. 12.

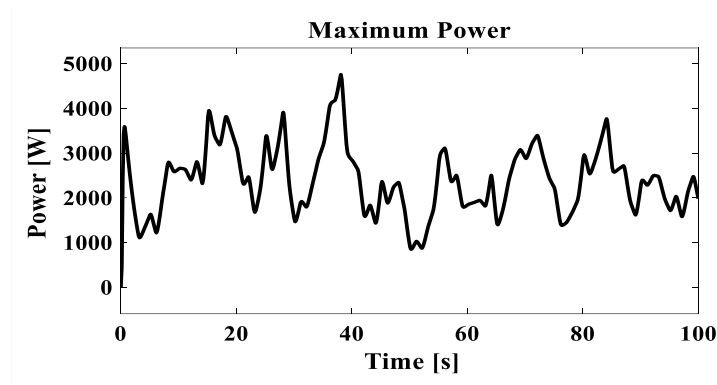


Fig. 9. Maximum power profile

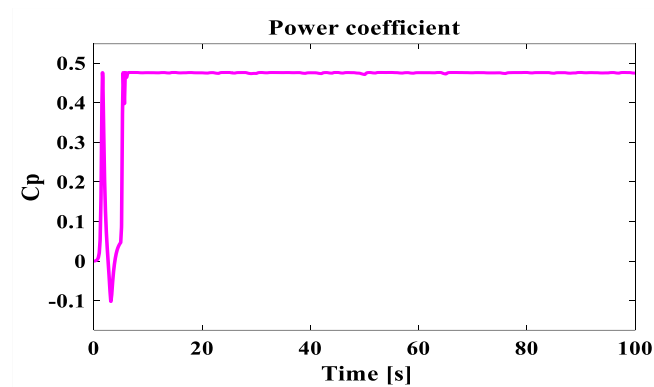


Fig. 10. Power coefficients

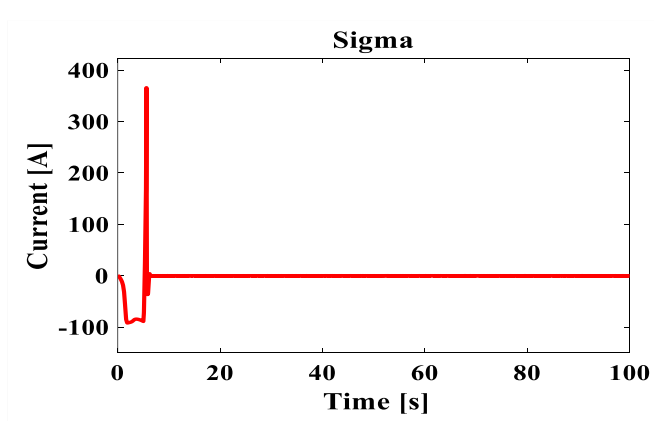


Fig. 11. Sliding surface about the reference

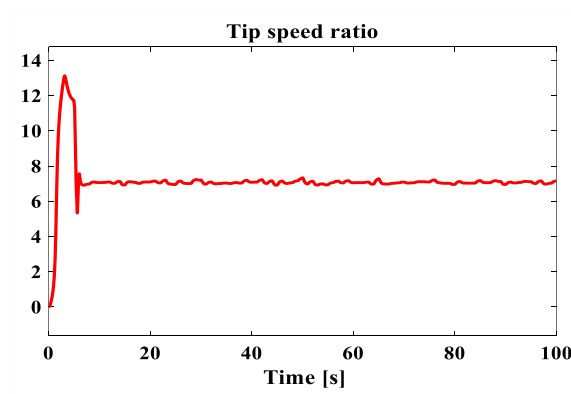


Fig. 12. Tip speed ratio

The performance of the generator by the application of the sliding mode controller is shown in Fig. 13 to Fig. 16. Fig. 3 shows a schematic diagram of the overall control configuration. The grid side control's goal is to keep the Back-to-Back converter's DC link voltage constant during wind variations when the set point is ($V_{DC} = 1200V$). This illustrates the DC-link voltage's resistance to wind fluctuations and is adjusted to settle around a continuous reference of 1200 V. Fig. 17 depicts the DC voltage. During the simulation, the DC voltage will obviously be changed within permissible limits in order to maintain the output voltage constant. Fig. 14 depicts 3-phase grid currents over time, while Fig. 13 depicts 3-phase grid voltages over time. The current increased as the wind speed increased, indicating that more active electricity was being injected into the grid.

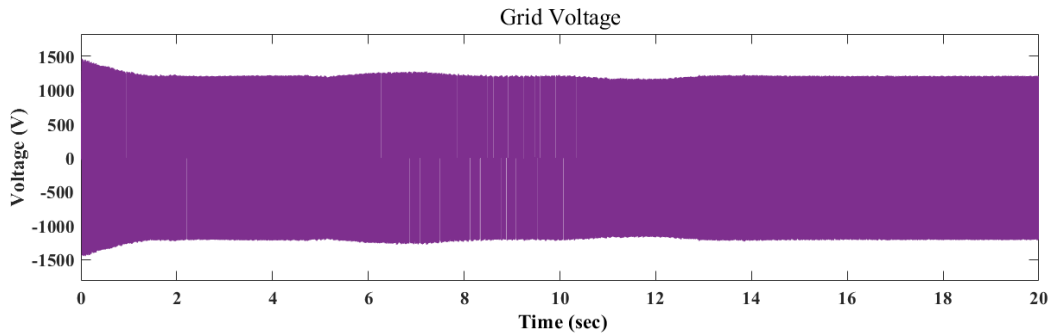


Fig. 13. Grid output voltage

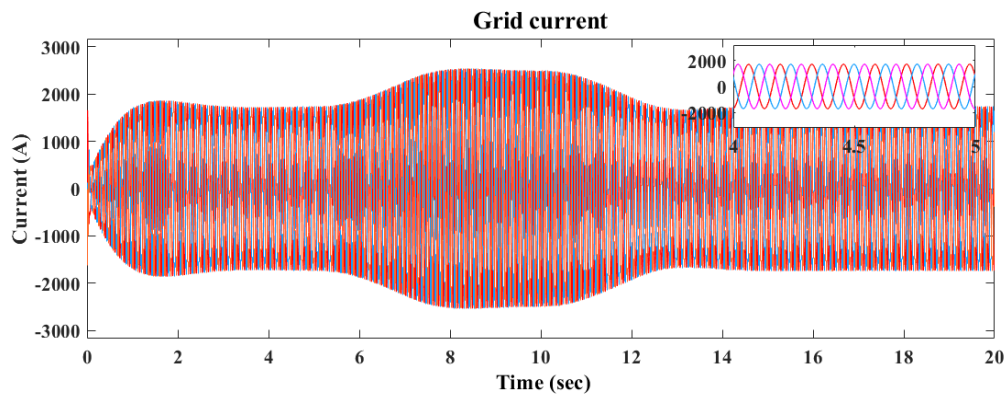


Fig. 14. Grid ABC current

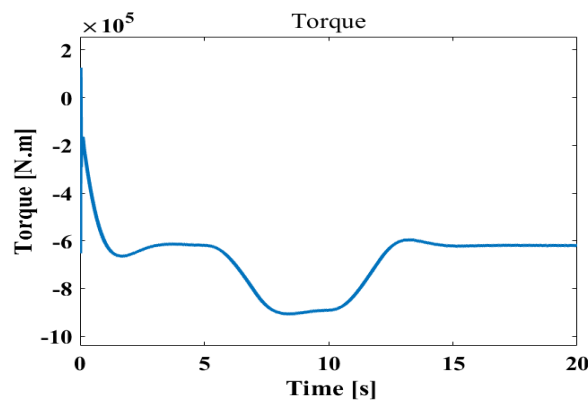


Fig. 15. Electromagnetic torque

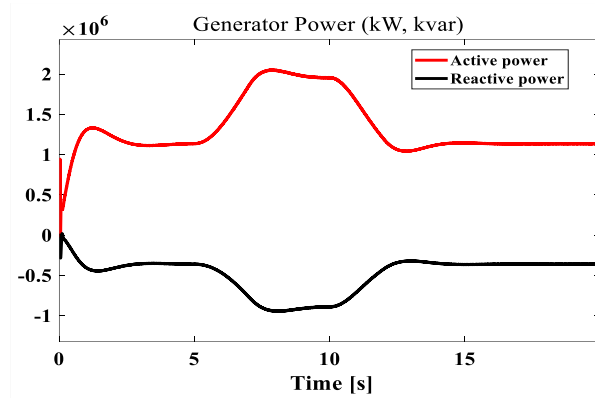


Fig. 16. Generator output power

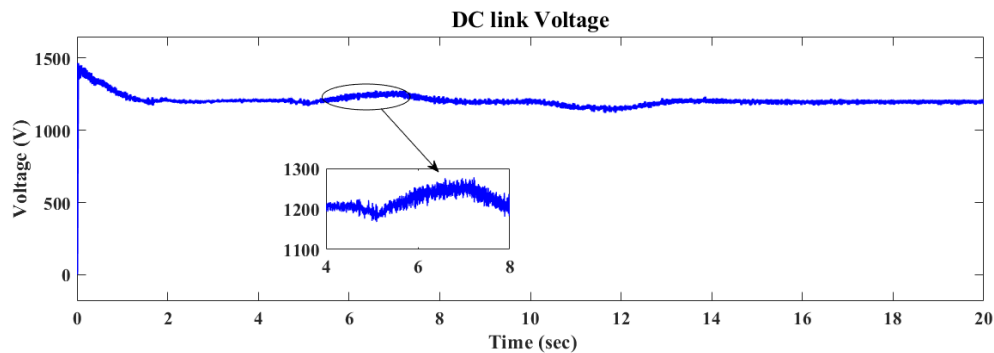


Fig. 17. DC link voltage

5. Conclusion

Presently, the wind energy industry is showing a tendency toward grid-connected wind turbine research and development. The following are the main concerns of today's wind turbine manufacturers: A medium-voltage direct-driven permanent magnet synchronous generator with variable speed technology and the creation of sophisticated control systems to improve wind energy conversion efficiency and meet grid code requirements. To validate the system, a fast response dynamic control via sliding mode with a modified super-twisting algorithm was constructed and simulated in this work. The control approach is higher-order sliding mode controls, which are used to regulate a nonlinear wind energy conversion system that causes mechanical wear when using first-order sliding mode controls. The study successfully decreased the chattering effect caused by the switching gain owing to the high activity of the control input. While the main principle of higher-order sliding mode controls is presented here, approaches that allow sliding mode controllers to operate at orders greater than 2 can be used to further reduce chattering. More work can be done to lead to the real implementation of higher-order sliding mode controllers by studying conditions such as loading, grid connections, and faults.

Author Contribution: All authors contributed equally to the main contributor to this paper. All authors read and approved the final paper.

Funding: This research received no external funding

Conflicts of Interest: The authors declare no conflict of interest.

References

- [1] H. H. H. Mousa, A. R. Youssef, and E. E. M. Mohamed, "Variable step size P&O MPPT algorithm for

- optimal power extraction of multi-phase PMSG based wind generation system,” *Int. J. Electr. Power Energy Syst.*, vol. 108, no. December 2018, pp. 218–231, 2019, <https://doi.org/10.1016/j.ijepes.2018.12.044>.
- [2] J. Liu, F. Zhou, C. Zhao, Z. Wang, and B. Aguirre-Hernandez, “A PI-type sliding mode controller design for PMSG-based wind turbine,” *Complexity*, vol. 2019, 2019, <https://doi.org/10.1155/2019/2538206>.
- [3] T. Adefarati and G. D. Obikoya, “Evaluation of wind resources potential and economic analysis of wind power generation in South Africa,” *Int. J. Eng. Res. Africa*, vol. 44, pp. 150–181, 2019, <https://doi.org/10.4028/www.scientific.net/JERA.44.150>.
- [4] Y. Charabi and S. Abdul-Wahab, “Wind turbine performance analysis for energy cost minimization,” *Renewables Wind. Water, Sol.*, vol. 7, no. 1, 2020, <https://doi.org/10.1186/s40807-020-00062-7>.
- [5] S. H. Qazi and M. W. Mustafa, “Review on active filters and its performance with grid connected fixed and variable speed wind turbine generator,” *Renew. Sustain. Energy Rev.*, vol. 57, no. 3, pp. 420–438, 2016, <https://doi.org/10.1016/j.rser.2015.12.049>.
- [6] S. Rhaili, A. Abbou, A. Ziouh, and R. Elidrissi, “Comparative study between PI and FUZZY logic controller in vector controlled five-phase PMSG based variable-speed wind turbine,” *Proc. - 2018 IEEE 12th Int. Conf. Compat. Power Electron. Power Eng. CPE-POWERENG 2018*, pp. 1–6, 2018, <https://doi.org/10.1109/CPE.2018.8372550>.
- [7] O. Apata and D. T. O. Oyedokun, “Wind turbine generators: Conventional and emerging technologies,” *Proc. - 2017 IEEE PES-IAS PowerAfrica Conf. Harnessing Energy, Inf. Commun. Technol. Afford. Electrification Africa, PowerAfrica 2017*, pp. 606–611, 2017, <https://doi.org/10.1109/PowerAfrica.2017.7991295>.
- [8] G. H. Kim, Y. J. Kim, M. Park, I. K. Yu, and B. M. Song, “RTDS-based real time simulations of grid-connected wind turbine generator systems,” *Conf. Proc. - IEEE Appl. Power Electron. Conf. Expo. - APEC*, vol. 2, no. 2, pp. 2085–2090, 2010, <https://doi.org/10.1109/APEC.2010.5433523>.
- [9] M. Q. Duong, K. H. Le, F. Grimaccia, S. Leva, M. Mussetta, and R. E. Zich, “Comparison of power quality in different grid-integrated wind turbines,” *Proc. Int. Conf. Harmon. Qual. Power, ICHQP*, pp. 448–452, 2014, <https://doi.org/10.1109/ICHQP.2014.6842779>.
- [10] S. Y. Kong, R. C. Bansal, and Z. Y. Dong, “Comparative small-signal stability analyses of PMSG-, DFIG- and SCIG-based wind farms,” *Int. J. Ambient Energy*, vol. 33, no. 2, pp. 87–97, 2012, <https://doi.org/10.1080/01430750.2011.640802>.
- [11] A. Kumar, S. Tomar, K. K. Gautam, and A. Lodhi, “Integration of SCIG Wind Energy Conversion Systems to the Grid,” *International Journal of Engineering Science Invention (IJESI)*, vol. 9, no. 6, pp. 28–36, 2020, [https://www.ijesi.org/papers/Vol\(9\)i6/Series-2/E0906022836.pdf](https://www.ijesi.org/papers/Vol(9)i6/Series-2/E0906022836.pdf).
- [12] A. Shahni, S. H. Qazi, G. S. Kaloi, and R. Ullah, “Review on Performance Analysis of SCIG and PMSG-Based Wind Energy Conversion System Systems,” *Int. J. Electron. Commun. Eng.*, vol. 6, no. 7, pp. 1–12, 2019, <https://doi.org/10.14445/23488549/IJECE-V6I7P101>.
- [13] M. T. Nafisa, E. Jahan, and M. A. Mannan, “Design and Analysis of a Grid-Tied Dual Rotor PMSG and SCIG-Based Wind Farms,” *2021 IEEE 9th Region 10 Humanitarian Technology Conference (R10-HTC)*, 2021, pp. 01–06, 2021, <https://doi.org/10.1109/R10-HTC53172.2021.9641607>.
- [14] O. J. Tola, E. S. Obe, and L. U. Anih, “Modeling and analysis of dual stator windings permanent magnet synchronous motor,” *IEEE 3rd International Conference on Electro-Technology for National Development (NIGERCON)*, 2017, pp. 861–871, <https://doi.org/10.1109/NIGERCON.2017.8281954>.
- [15] M. Abbes, I. Mehouchi, and S. Chebbi, “Improved VSM control of PMSG-based wind farms for transient stability enhancement,” *Turkish J. Electr. Eng. Comput. Sci.*, vol. 27, no. 1, pp. 274–288, 2019, <https://doi.org/10.3906/elk-1806-17>.
- [16] S. Sharma and G. K. Banerjee, “Performance Analysis of Permanent Magnet Synchronous Generator Driven by Wind Turbines,” *Advance Res. Innov. Sci. Eng.*, p. EC-24, 2014, <https://www.researchgate.net/profile/Samraat-Sharma/publication/358376312>.
- [17] M. Devika, R. Geetha, and G. Hemalatha, “A Review on Power Converter Topology for Wind Energy

- System for Permanent Magnet Synchronous Generator,” *International Journal of Electronics Communication and Computer Engineering*, vol. 8, no. 1, 2017, https://ijecce.org/administrator/components/com_jresearch/files/publications/IJECCE-4052-FINAL.pdf.
- [18] A. Merabet, A. A. Tanvir, and K. Beddek, “Speed control of sensorless induction generator by artificial neural network in wind energy conversion system,” *IET Renew. Power Gener.*, vol. 10, no. 10, pp. 1597–1606, 2016, <https://doi.org/10.1049/iet-rpg.2016.0285>.
- [19] I. W. Jeong, W. S. Choi, and K. H. Park, “Sensorless vector control of induction motors for wind energy applications using MRAS and ASO,” *J. Electr. Eng. Technol.*, vol. 9, no. 3, pp. 873–881, 2014, <https://doi.org/10.5370/JEET.2014.9.3.873>.
- [20] M. Aimene, A. Payman, and B. Dakyo, “Comparative Study between Flatness-Based and Field-Oriented Control Methods of a Grid-Connected Wind Energy Conversion System,” *Processes*, vol. 10, no. 2, p. 378, 2022, <https://doi.org/10.3390/pr10020378>.
- [21] C.-T. Ma and Z.-H. Shi, “A Distributed Control Scheme Using SiC-Based Low Voltage Ride-Through Compensator for Wind Turbine Generators,” *Micromachines*, vol. 1, no. 39, 2021, <https://doi.org/10.3390/mi13010039>.
- [22] N. Hawkins, B. Bhagwat, and M. L. McIntyre, “Nonlinear current-mode control of scig wind turbines,” *Energies*, vol. 14, no. 1, 2021, <https://doi.org/10.3390/en14010055>.
- [23] J. Iqbal, M. Ullah, S. G. Khan, B. Khelifa, and S. Ćuković, “Nonlinear control systems - A brief overview of historical and recent advances,” *Nonlinear Eng.*, vol. 6, no. 4, pp. 301–312, 2017, <https://doi.org/10.1515/nleng-2016-0077>.
- [24] N. El Ouanjli, A. Derouich, A. El Ghzizal, S. Motahhir, A. Chebabhi, Y. El Mourabit, and M. Taoussi, “Modern improvement techniques of direct torque control for induction motor drives - a review,” *Prot. Control Mod. Power Syst.*, vol. 4, no. 11, 2019, <https://doi.org/10.1186/s41601-019-0125-5>.
- [25] H. Hamla, L. Rahmani, and N. Belhaouchet, “A modified direct torque control with minimum torque ripple and constant switching frequency for induction motor drives,” *Int. Trans. Electr. Energy Syst.*, vol. 29, no. 12, pp. 1–20, 2019, <https://doi.org/10.1002/2050-7038.12120>.
- [26] P. D. Patel and S. N. Pandya, “Comparative Analysis of Torque Ripple for Direct Torque Control based Induction Motor Drive with different strategies,” *Aust. J. Electr. Electron. Eng., Taylor Fr.*, 2022, <https://doi.org/10.1080/1448837X.2021.2023249>.
- [27] E. G. Shehata, “Sliding mode direct power control of RSC for DFIGs driven by variable speed wind turbines,” *Alexandria Eng. J.*, vol. 54, no. 4, pp. 1067–1075, 2015, <https://doi.org/10.1016/j.aej.2015.06.006>.
- [28] G. S. Kaloi, J. Wang, and M. H. Baloch, “Active and reactive power control of the doubly fed induction generator based on wind energy conversion system,” *Energy Reports*, vol. 2, pp. 194–200, 2016, <https://doi.org/10.1016/j.egyr.2016.08.001>.
- [29] S. M. Hosseini and M. Manthouri, “Type 2 adaptive fuzzy control approach applied to variable speed DFIG based wind turbines with MPPT algorithm,” *Iranian Journal of Fuzzy Systems*, vol. 19, no. 1, pp. 31–45, 2022, <https://dx.doi.org/10.22111/ijfs.2022.6549>.
- [30] J. Tavoosi, A. Mohammadzadeh, B. Pahlevanzadeh, M. B. Kasmani, S. S. Band, R. Safdar, and A. H. Mosavi, “A machine learning approach for active/reactive power control of grid-connected doubly-fed induction generators,” *Ain Shams Eng. J.*, vol. 13, no. 2, 2022, <https://doi.org/10.1016/j.asej.2021.08.007>.
- [31] Y. Huang, “Sliding Mode Observer Design for Permanent Magnetic Synchronous Generator Based Wind Energy Conversion Systems,” *Southern Illinois University at Edwardsville*, 2017, <https://www.proquest.com/docview/1899625348>.
- [32] H. Mamur, “Design, application, and power performance analyses of a micro wind turbine,” *Turkish J. Electr. Eng. Comput. Sci.*, vol. 23, pp. 1619–1637, 2015, <https://doi.org/10.3906/elk-1401-174>.
- [33] O. Tola and E. A. Umoh, “Modeling and analysis of a permanent magnet synchronous generator dedicated to wind energy conversion,” *2nd International Engineering Conference (IEC 2017)*, 2017,

- pp. 216–225, <http://repository.futminna.edu.ng:8080/jspui/handle/123456789/6974>.
- [34] T. Shi, L. Shi, and L. Yao, "Detailed modelling and simulations of an all-DC PMSG-based offshore wind farm," *J. Eng.*, vol. 2019, no. 16, pp. 845–849, 2019, <https://doi.org/10.1049/joe.2018.8403>.
- [35] K. Tazi, M. F. Abbou, and F. Abdi, "Performance analysis of micro-grid designs with local PMSG wind turbines," *Energy Systems*, vol. 11, no. 3, pp. 607–639, 2020, <https://doi.org/10.1007/s12667-019-00334-2>.
- [36] E. A. Umoh and O. J. Tola, "Electronic circuit realization and adaptive control of a chaotic permanent magnet synchronous motor," *2nd International Engineering Conference (IEC 2017)*, 2017, pp. 395–404, <http://repository.futminna.edu.ng:8080/jspui/handle/123456789/6857>.
- [37] O. J. Tola, E. A. Umoh, and E. A. Yahaya, "Pulse Width Modulation Analysis of Five-Level Inverter-Fed Permanent Magnet Synchronous Motors for Electric Vehicle Applications," *Int. J. Robot. Control Syst.*, vol. 1, no. 4, pp. 477–487, 2021, <https://doi.org/10.31763/ijrcs.v1i4.483>.
- [38] A. G. Sanchez, M. G. Molina, and A. M. Rizzato Ledo, "Dynamic model of wind energy conversion systems with PMSG-based variable-speed wind turbines for power system studies," *Int. J. Hydrogen Energy*, vol. 37, no. 13, pp. 10064–10069, 2012, <https://doi.org/10.1016/j.ijhydene.2011.12.077>.
- [39] P. Xing, L. Fu, G. Wang, Y. Wang, and Y. Zhang, "A compositive control method of low-voltage ride through for PMSG-based wind turbine generator system," *IET Gener. Transm. Distrib.*, vol. 12, no. 1, pp. 117–125, 2018, <https://doi.org/10.1049/iet-gtd.2017.0270>.
- [40] H. Sun, Y. Han, and L. Zhang, "Maximum Wind Power Tracking of Doubly Fed Wind Turbine System Based on Adaptive Gain Second-Order Sliding Mode," *J. Control Sci. Eng.*, vol. 18, no. 5342971, 2018, <https://doi.org/10.1155/2018/5342971>.
- [41] H. Benbouhenni, F. Mehedi, and L. Soufiane, "New direct power synergetic-SMC technique based PWM for DFIG integrated to a variable speed dual-rotor wind power," *Automatika*, vol. 63, no. 4, pp. 718–731 2022, <https://doi.org/10.1080/00051144.2022.2065801>.
- [42] R. Hiremath and T. Moger, "LVRT enhancement of DFIG-driven wind system using feed-forward neuro-sliding mode control," *Open Eng.*, vol. 11, no. 1, pp. 1000–1014, 2021, <https://doi.org/10.1515/eng-2021-0100>.